

Reitveld refinement, structural, optical band gap and low-temperature magnetic characterization of Gd³⁺ doped spinel cubic CoFe₂O₄ nanoparticles

A. Kumar^{1*}, M. K. Gora¹, S. Kumar¹, B. L. Choudhary², P. K. Maheshwari³ and S. N. Dolia¹

¹Department of Physics, University of Rajasthan, Jaipur-302004, Rajasthan, India

²Department of Physics, Banasthali Vidyapith, Banasthali-304022, Rajasthan, India

³Center for Non-Conventional Energy Resources, University of Rajasthan, Jaipur-302004, Rajasthan, India

Abstract

The current study unravels the structural, optical band gap and magnetic characteristics of rare-earth (RE) gadolinium (Gd) substituted CoGd_xFe_{2-x}O₄ (x= 0.00 - 0.10, in the interval of 0.02) nanocrystallites synthesized by the sol-gel self-ignition route. The XRD analysis and Rietveld refinement confirmed the existence of a single cubic phase with a crystallite size of ~15-21 nm range, further confirmed by HRTEM results. SEM images confirmed the well-known nano-size morphology for all the samples. The magnetization measurements show a hard ferromagnetic nature for all specimens within the temperature range of 20-300K. Coercivity, remanent, and saturation magnetization monotonically increased with a reduction in temperature from 300K to 20K. UV-Vis absorbance results show that the band gap energy of CoFe₂O₄ nanoparticles (NPs) decreases with increasing Gd³⁺ ion doping and have band gap energy values of 2.47, 2.15, 2.02, 2.00, 1.43 and 1.95 eV for x= 0.00, 0.02, 0.04, 0.06, 0.08, 0.10, respectively in CoGd_xFe_{2-x}O₄ nanoferrites. The present study reveals that structural, optical band gap and magnetic properties could be altered by monitoring the quantity of gadolinium in cobalt nanoferrites.

Received: 07 August 2022

Revised: 23 August 2022

Accepted: 23 August 2022

DOI: <https://doi.org/10.3329/bjisir.v57i3.62019>

Keywords: Nanoferrites; Rare earth doping; Hard ferromagnet; Saturation magnetization; Coercivity; Optical band gap

Introduction

Spinel ferrites are around the clock, drawing researchers' attention due to their flexible structural, electromagnetic properties and can be used in enormous applications of engineering and technology at a very reasonable cost (Amiri *et al.*, 2019; Goldman, 1999; Palnisamy *et al.*, 2019; Reddy *et al.*, 2016; Valenzuela, 2012). Spinel ferrites at the nano-level offer several advantages over their bulk equal through the improved surface-to-volume (S/V) ratio. The increased S/V ratio in NPs leads to enhancement in various properties like thermal, electrical, mechanical, magnetic and optical characteristics in spinel ferrites. As the S/V ratio is linearly correlated to particle size and resultant, it plays a significant part in determining magneto-electric properties

like anisotropy, saturation magnetization, and dielectric properties (Issa *et al.*, 2013; Jahan *et al.*, 2021).

Moreover, nanocrystalline ferrites possess high chemical stability and high transition temperatures. Nanoferrites are also observed as suitable recyclable materials and have good compatibility with living systems. Because of that, nanoferrites are being utilized in many applications in water remediation such as photocatalysis, electronic and magnetic devices like microwave filters, power supplies, radiofrequency coils, transfer cores in high-frequency microwave instruments, storage devices, and sensors (Dippong *et al.*, 2021; Schloemann, 2000).

*Corresponding author e-mail: amkanisk@gmail.com

The utilities of ferrites in designing and producing recent eco & handy magnetic devices and carriers are highly dependent upon the cation distribution and electronic and magnetic structures of spinel ferrites. Many research papers have been published on different platforms on ferrites; however, cobalt ferrite is a strong candidate due to having significant assets, for instance, raised coercivity, giant magnetocrystalline anisotropy, high saturation magnetization, with broad uses in technological and electrical fields. Cobalt ferrite is the most adjustable hard ferrite since its presentation can be significantly changed by lattice integration with different metals, with a partially inverse spinel structure having an $Fd\bar{3}m$ space group (Menezes *et al.*, 2019; Zeng *et al.*, 2017; Parvin *et al.*, 2020). Co based spinels provide a perfect platform of reasonable, simply scalable electrocatalysts. More enhancement in the different electromagnetic and chemical properties can be done by presenting metal and oxygen ion vacancies (Debnath *et al.*, 2020).

Previously many researchers have done colossal work on the consequence of assimilation of RE trivalent ions in cobalt ferrites. One group of researchers prepared different RE-doped Co nanoferrites and found that saturation magnetization was reduced by adding rare earth metal ions in Co nanoferrites (Dhiman and Singhal 2019). Gd-doped Co nanoferrites were synthesized by another research group and informed that as the gadolinium content increased, the coercivity was improved, the saturation magnetization diminished, and magnetocrystalline anisotropy constant was improved due to crystallite dimensions effect and ions dispersal (Murugesan *et al.*, 2015). The structural and transport behavior of Gd^{3+} doped Co nanoferrites were studied and found to have high resistivity, slight dielectric loss and soft magnetic behavior due to Gd^{3+} substitution (Pervaiz and Gul 2012). Adding Gd^{3+} in ferrite structures results in abnormalities similar to an increase in lattice boundary or microstrain owing to ionic radius inconsistency (Sharma *et al.*, 2021), which causes strain and suggestively alters the structural and transport characteristics. In continuation, Q. Lin *et al.*, study the structural and magnetic properties of $CoGd_xFe_{2-x}O_4$ ($x=0.00, 0.04, 0.08$) NPs (Lin *et al.*, 2015). M-H Curve recorded at RT only up to 1 tesla applied magnetic fields and M-T magnetization was not recorded. So, there is a need to investigate the magnetic properties of Gd-doped $CoFe_2O_4$ nanoferrites at the higher applied magnetic field and field-temperature-dependent magnetic measurements to understand the magnetization of Gd-doped $CoFe_2O_4$ NPs. Hence, the impression of Gd^{3+} ions assimilation on cobalt ferrite's structural and magnetic behavior is worth investigating.

Instead, nanoferrites can be effortlessly prepared using standard procedures, such as the microwave refluxing technique, a

hydrothermal method, decomposition way, sol-gel self-combustion route and chemical coprecipitation method (Su *et al.*, 2014; Satyanarayana *et al.*, 2003; Mykhailovych, 2021; Samariya *et al.*, 2013; Kumar *et al.*, 2015; Klein *et al.*, 2018). We have selected the sol-gel auto-combustion method for producing nanoferrites because it is equated to other producing methods; this process is an economical, time and energy-saving technique for getting the comparatively even size of ferrite NPs (Klein *et al.*, 2018).

This article's main work explored the significance of gadolinium ion assimilation in $CoFe_2O_4$ and its impact on the structural, optical band gap and magnetic properties. Gd^{3+} ions substitution influenced the cobalt nanoferrites by replacing the Fe ion in the fcc unit cell, which were investigated by analyzing different characterizations. Here, we first confirmed the successful doping of Gd in Co ferrite nanocrystals by XRD, SEM followed by HRTEM images in addition to typically selected area electron diffraction (SAED) patterns, and then studied various extravagant features intensely and systematically. SQUID magnetometry technique was employed to find magnetic parameters like saturation magnetization, coercivity and retentivity at room temperature and below temperatures. UV-Vis spectroscopy measurements were done to analyze the optical band gap of synthesized nanoferrites samples. These analyzed properties will enhance the utility of synthesized NPs in science and technological fields.

Furthermore, it was shown here that the structure and magnetic properties were interrelated. Remarkably, our results established striking improvement in the magnetic and optical band gap characteristics of $CoGd_xFe_{2-x}O_4$ nanoferrites compared to their complement undoped $CoFe_2O_4$ nanoferrites.

Materials and methods

$CoGd_xFe_{2-x}O_4$ ($x = 0.0-0.10$, in an interval of 0.02) nanocrystallites samples have been prepared by the sol-gel self-combustion method. Sigma-Aldrich brand having a great purity analytical grade Co, Fe, Gd nitrates and $C_6H_8O_7$ have been used as initial materials. $C_6H_8O_7$ was taken in 3:1 to the metal nitrates in weight. Different metal nitrate solutions were completed by dissolving them in distilled water. After that, all solutions were taken in a single vessel and stirred at high speed to attain a consistent solution. Then, the $C_6H_8O_7$ solution was transferred into the mixed solution of metal nitrates with continuous mixing. The pH of the mixer was held above eight through accumulating NH_4OH throughout the method. The combined mixed solution was held at the oven's constant temperature ($80^\circ C$) with continued stirring.

In about five hours, the solution becomes changed into a pasty gel. Afterward, the temperature was elevated to 130 °C before starting the self-combustion procedure. The pasty gel converts into powder by freeing the organic deposit and fumes. This sample was put in a furnace for a day at 300°C for dehydration. All six samples were prepared in a similar experimental state (Chejara *et al.*, 2022; Patta *et al.*, 2021; Riaz *et al.*, 2022).

Detection method

The phase purity has been established by X-ray diffraction (XRD, Panalytical make X'Pert PRO system Diffractometer) with $\text{CuK}\alpha$ line source ($\lambda = 1.5406 \text{ \AA}$) at room temperature. Diffractograms with diffraction intensity versus Bragg's diffraction angle (2θ) were recorded between 10° to 70° (2θ). Further, XRD data has been analyzed with Rietveld refinement using the Fullprof software tool. To understand the morphology of synthesized nanoferrites, SEM measurements were carried out on a ZEISS-made electron microscope. A high-resolution transmission electron microscope examined particle size (HRTEM, TecnaiTM G2 20); the samples (a pinch) were dispersed in ethanol and sonicated for an hour. After sonication, a drop of the solution using the syringe was mounted on the carbon-coated copper grid. The grid was air-dried for about half an hour before the measurement. Magnetic hysteresis was measured at 20, 100, 200, and 300 K using a SQUID (Quantum Design MPMS-3), changing magnetic fields from 50 kOe to 50 kOe. Further, field cooled (FC) and zero fields cooled (ZFC) data were recorded with an external used magnetic field of 100, 500, and 1000 Oe in the temperature limit of 10–300 K. UV-Vis spectroscopy data measurement for analyzing optical band gap was done by Shimadzu UV-2600 spectrophotometer in the wavelength range of 200 nm to 800 nm.

Results and discussion

XRD analysis

The primary structural characterization technique (XRD) is used to examine the phase purity, crystallographic structure, crystal size, and lattice parameters as synthesized $\text{CoGd}_x\text{Fe}_{2-x}\text{O}_4$ ($x=0.0-0.10$, in an interval of 0.02) nanoferrites at 300K. XRD diffractograms have been recorded for the $\text{CoGd}_x\text{Fe}_{2-x}\text{O}_4$ nanoferrites series with the 2θ range of 10° to 70° , presented in figure 1a. This figure concludes the phase purity of the studied nanoferrites specimens, as all the diffraction peaks are perfectly matched with characteristic XRD patterns of CoFe_2O_4 nanoferrites, which is exhibited in the cubic spinel crystalline structure within the space group

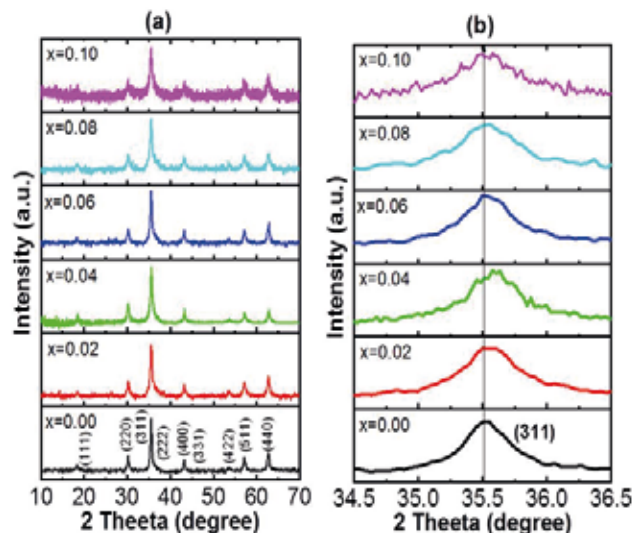


Fig. 1(a). XRD plots of $\text{CoGd}_x\text{Fe}_{2-x}\text{O}_4$ ($x = 0.0, - 0.10$, in an interval of 0.02) ferrite NPs at room temperature, **(b)** Enlarged view of the (311) peak shift with diffraction angle

of $\text{Fd}\bar{3}m$ (JCPDS file no. 22–1086) (Naik and Hasolkar 2020). Furthermore, it can also be concluded that with doping of Gd in cobalt nanoferrites, no additional intensity peak is detected in the XRD pattern, which attributes successful doping of larger radius Gd^{3+} in the cobalt ferrites structure (John *et al.*, 2020). The high-intensity peaks were observed at about 2θ values of 18.380, 30.260, 35.700, 43.240, 53.570, 57.200, and 62.790, indexed as (111), (220), (311), (400), (422), (511), and (440) planes respectively. Gd^{3+} ions in the samples preferably reside in the octahedral (B) site. Moreover, figure 1(b) showed the (311) peak's zoomed sight in the 2θ angle from 34.5° to 36.5° of the $\text{CoGd}_x\text{Fe}_{2-x}\text{O}_4$ nanoferrites series, and it can be concluded from figure 1b that the uppermost intense peak is moved in the direction of larger Bragg angle with Gd doing in cobalt nanoferrites.

For more structural analysis, Rietveld refinement of XRD data was performed to evaluate the lattice parameters, crystal size, and density of these nanoferrites samples using Fullprof software (Lal *et al.*, 2019). Figure 2(a-f) displays the fitted Rietveld refinement XRD patterns of $\text{CoGd}_x\text{Fe}_{2-x}\text{O}_4$ ($x=0.0 - 0.10$, in an interval of 0.02) nanoferrites. As shown in figure 2(a-f), it is concluded that the Rietveld fitted patterns (solid red lines) were perfectly matched with the experimentally observed diffraction patterns (black points) for all the studied samples. It can also be verified with the value of χ^2 (Fitting parameter), as the obtained value of χ^2 in Rietveld refinement is found in single-digit (displayed in Table I), which confirms

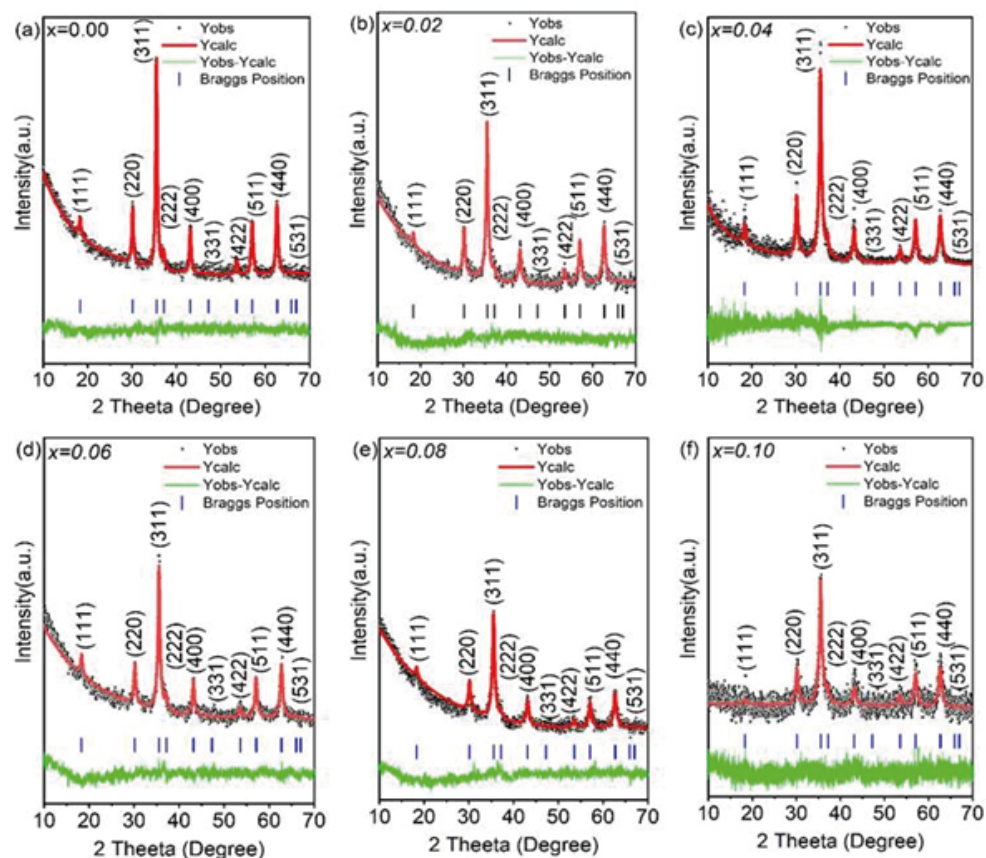


Fig. 2. Rietveld fitted XRD patterns of $\text{CoGd}_x\text{Fe}_{2-x}\text{O}_4$ nanoferrites; (a) $x = 0.00$, (b) $x = 0.02$, (c) $x = 0.04$, (d) $x = 0.06$, (e) $x = 0.08$ and (f) $x = 0.10$ ferrite NPs. Observed data is shown by black dots and red solid line is the calculated profile and the lower plot (green) is the intensity difference curve. Bragg peak positions are marked by vertical blue lines

Table I. Structural parameters and agreement factors for $\text{CoGd}_x\text{Fe}_{2-x}\text{O}_4$ nanoferrites

Gd Conc. (x)	Lattice parameter a (Å)	Unit cell volume V (Å ³)	Oxygen positional parameter (u)	χ^2	Bragg R - factor	Crystallite size (t) (nm)	d_x (gm/cm ³)
0.00	8.3750	587.4	0.2503	1.42	8.58	14.0	5.31
0.02	8.3862	589.7	0.2545	1.23	16.8	11.2	5.92
0.04	8.3723	586.8	0.2581	1.84	13.3	10.8	5.12
0.06	8.3792	588.3	0.2568	1.31	12.1	11.1	5.72
0.08	8.3837	589.2	0.2556	1.41	26.1	10.1	5.49
0.10	8.3845	589.4	0.2517	1.07	13.2	6.7	4.88

the goodness of fitting the experimental data. Respectable fitting of peak position and intensity with reasonable values of fitting parameters (χ^2 and Bragg R factor) confirmed the single-phase parameters, the volume of a unit cell, and fitting parameters of $\text{CoGd}_x\text{Fe}_{2-x}\text{O}_4$ are displayed in Table I.

Additionally, the average size (t) of pure and Gd doped CoFe_2O_4 nanocrystallites has been evaluated by the standard Debye–Scherrer formula, as revealed below (Cullity and Stock, 1978).

$$t = \frac{0.9 \lambda}{\beta \cos \theta}$$

where ' λ ' represents the wavelength of the X-ray diffractometer (CuK_α source, i.e., 1.5406 Å), ' β ' represents the FWHM of the Bragg's diffraction peaks, and ' θ ' represents the Bragg angle agreeing to that peak. Thus, crystallite sizes are calculated by taking the average crystalline size, corresponding to their respective 2θ and FWHM for all the nanoferrites samples. The observed average crystalline size is given in Table I for all the studied samples. Further, the X-ray density

(d_x) is obtained by the formula (Anwar *et al.*, 2021)

$$d_x = \frac{8M}{Na^3}$$

where ' a ' represents the fcc unit cell parameter, N represents Avogadro's number, and M represents the sample's relative molecular mass. Calculated crystallite size and density amplitudes are displayed in Table I for all the studied nanoferrites.

As shown in Table I, the average crystallite sizes decrease with a rise in Gd^{3+} concentration in Co Ferrite, which the following facts could explain. First, because of the greater ionic radius of Gd^{3+} ion (0.938 Å) equated to Fe^{3+} ion (0.645 Å), the substitution of Gd^{3+} in place of Fe^{3+} in CoFe_2O_4 leads to lattice strain which produces internal stress. The internal stress tries to stop the growth of NPs, resulting in a lessening

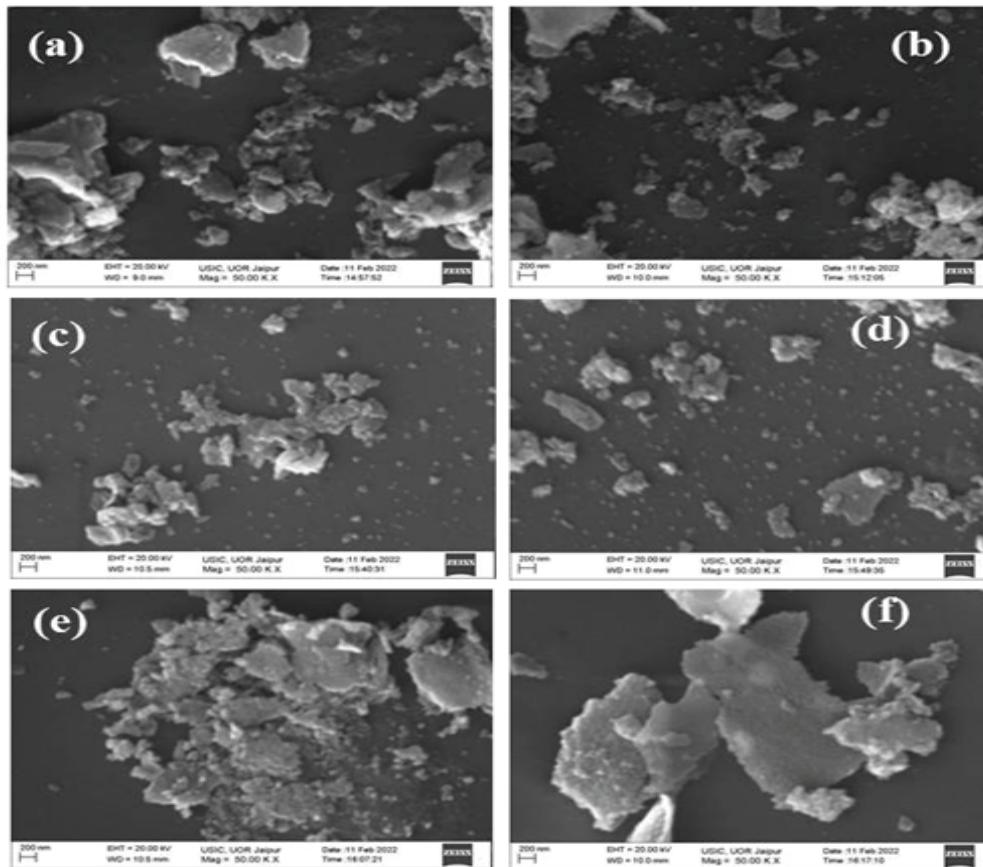


Fig. 3. SEM analysis of $\text{CoGd}_x\text{Fe}_{2-x}\text{O}_4$ nanoferrites; (a) $x = 0.0$, (b) $x = 0.02$, (c) $x = 0.04$, (d) $x = 0.06$, (e) $x = 0.08$ and (f) $x = 0.10$ ferrites NPs at 200 nm resolution with 50 KX magnification factor

crystalline size with growth in Gd^{3+} concentration in Co ferrite. Further, it is reported that more energy is required to form a Gd-O bond compared to a Fe-O bond. Hence, more energy is needed in crystallization, and growing NPs in Gd substituted ferrites than undoped ferrite (Zhao *et al.*, 2006).

SEM analysis

Moreover, the morphology of as-synthesized cobalt nanocrystals is illustrated by SEM micrographs at room temperature. Figure 3(a-f) depicts the SEM micrographs of $\text{CoGd}_x\text{Fe}_{2-x}\text{O}_4$ ($x=0$ to 0.1, $\Delta x=0.02$) nanoferrites series. SEM

(Carl-Zeiss EVO 18) analysis has been executed at a high resolution of 200 nm with a 50 KX magnification factor. SEM micrographs clearly show that cobalt nanoferrites and Gd doped cobalt nanoferrites have asymmetrical morphology and un-prominent grain boundaries. Agglomeration is also observed in certain particles because of magnetic interaction among particles (Jiang and Yang, 2009). The cluster of particles is extra noticeable in Gd doped nanoferrites particles. It may be because of the deposition of Gd^{3+} ions at grain boundaries. Due to this aggregation, a reduction in particle size occurred with Gd doping in cobalt nanoferrites, further confirming the crystallite size estimated from XRD

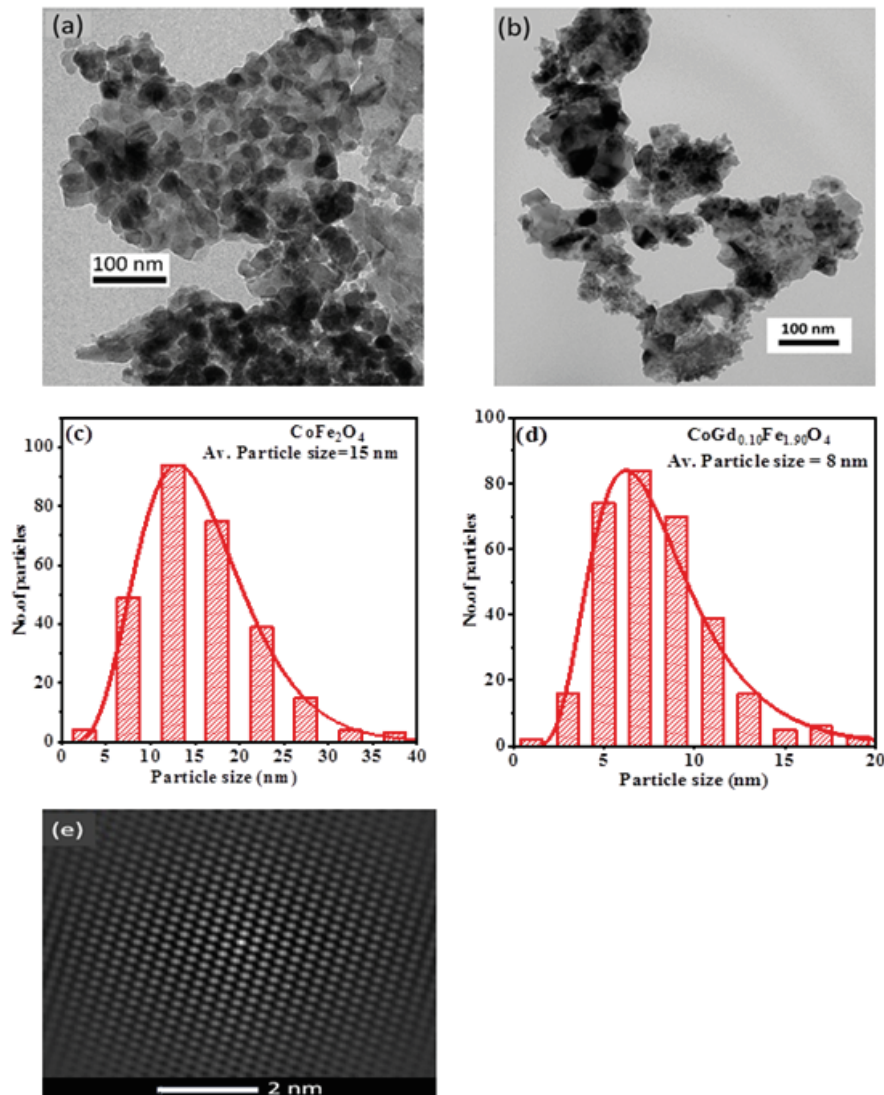


Fig. 4. HRTEM analysis of nanoferrites; (a) HRTEM micrograph of CoFe_2O_4 , (b) HRTEM micrograph of $\text{CoGd}_{0.10}\text{Fe}_{1.90}\text{O}_4$, (c) fitted histograms for CoFe_2O_4 , (d) fitted histograms for $\text{CoGd}_{0.10}\text{Fe}_{1.90}\text{O}_4$, (e) HRTEM micrograph of CoFe_2O_4 at 2 nm resolution

outcomes. The average particle size obtained from all the studied specimens by SEM analysis is in the nm range, confirming the successful formation of NPs.

HRTEM analysis

The additional information about the structure and morphology of $\text{CoGd}_x\text{Fe}_{2-x}\text{O}_4$ nanoferrites are exemplified by the HRTEM microstructural analysis, shown in figure 4. HRTEM micrographs depict the formation of very crystalline ferrites NPs with variable crystal size and shape. Strong agglomeration tendency of the particles, clearly noticeable in HRTEM micrographs (figure 4a and figure 4b), which further agree to SEM microstructural images. Higher agglomeration

is a general tendency of nanoferrites by reason of robust inter-particle interaction (Valenzuela, 2012). Additionally, the average crystallite sizes were obtained by the size dispersal histogram fitted with a Gaussian function for CoFe_2O_4 and $\text{CoGd}_{0.10}\text{Fe}_{1.90}\text{O}_4$ nanoferrites exposed in figure 4c and figure 4d, correspondingly. The synthesized nanocrystallite size varied within the 2-40 nm range and looked like a spherical type shape. The average crystalline size is 15 nm and 8 nm for CoFe_2O_4 and $\text{CoGd}_{0.10}\text{Fe}_{1.90}\text{O}_4$ nanoferrites, respectively, using a size distribution histogram, which is in good agreement with that obtained through the Debye-Scherrer formula using XRD data.

It can also be concluded with the size distribution histogram

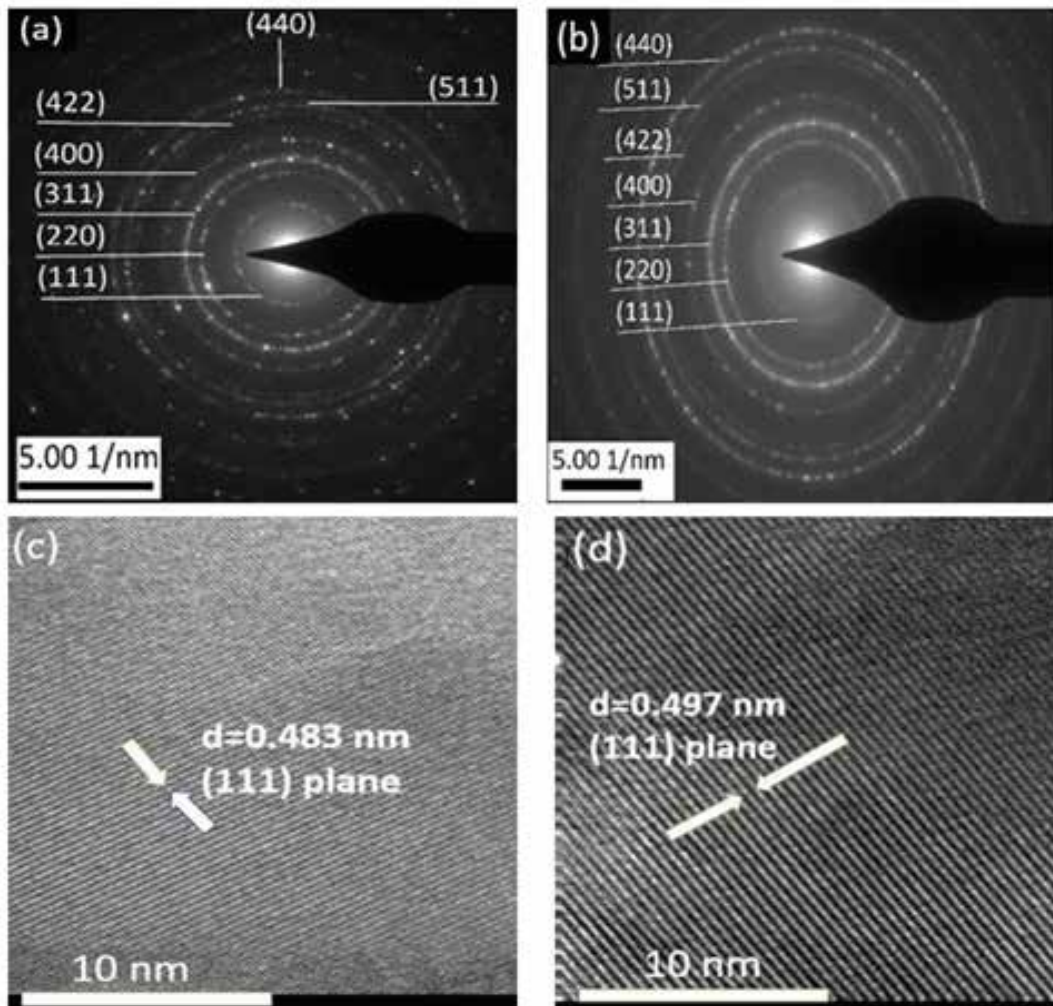


Fig. 5. Selected Area Electron Diffraction (SAED) patterns of $\text{CoGd}_x\text{Fe}_{2-x}\text{O}_4$; (a) $x=0.00$, (b) $x=0.10$, (c) TEM micrograph of CoFe_2O_4 at 10 nm resolution, obtained d_{hkl} corresponds to (111) plane and (d) TEM micrograph of $\text{CoGd}_{0.10}\text{Fe}_{1.90}\text{O}_4$ at 10 nm resolution, obtained d_{hkl} corresponds to (111) plane

that crystalline size is reduced with Gd doping in cobalt nanoferrites, which is further in excellent agreement with the XRD result. Moreover, a 2 nm resolution HRTEM micrograph of CoFe_2O_4 nanoferrites confirmed the absence of any defects in the sample at an atomic level, see figure 4e. Figures 5a and 5b present the bright, distinctive selected area electron diffraction (SAED) ring pattern of CoFe_2O_4 and

$\text{CoGd}_{0.10}\text{Fe}_{1.90}\text{O}_4$ nanoferrites, respectively. These SAED patterns of studied nanoferrites contain concentric rings with irregular spots. These bright spots correspond to confirm the crystalline nature of nanoferrites. These concentric rings are also index-able (like XRD) and marked correspond to (111), (220), (311), (400), (422), (511) and (440) Bragg planes, agreed to the spinel ferrite fcc crystal structure within $\text{Fd}\bar{3}m$

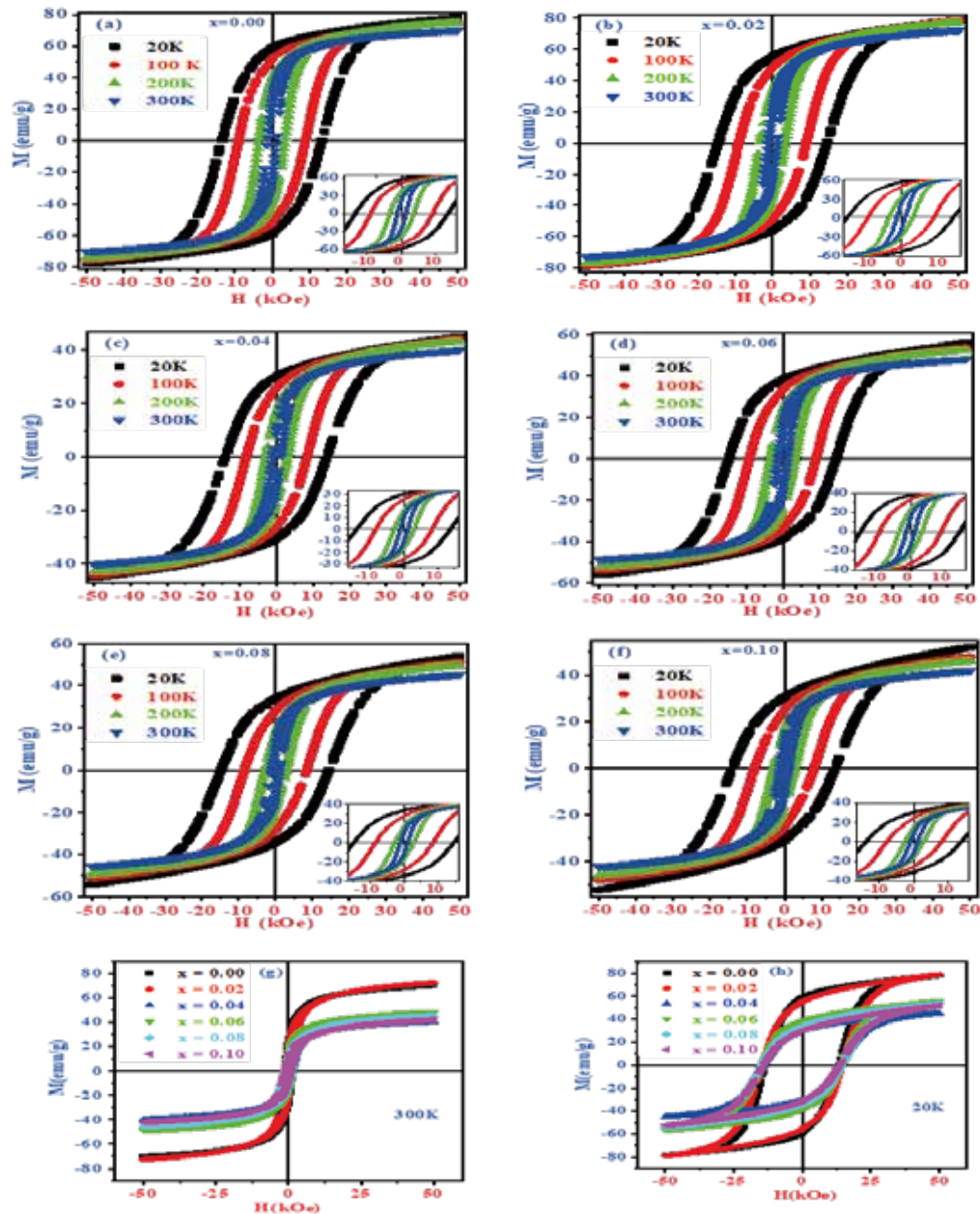


Fig. 6 (a-f). Magnetization (M) versus applied magnetic field (H) hysteresis loop of $\text{CoGd}_x\text{Fe}_{2-x}\text{O}_4$ ($x = 0.00-0.10$, step size 0.02), measured at different shown temperatures and Expanded view shown in insets, (g-h) for various Gd^{3+} ions concentrations at temperatures 300K and 20K, respectively

space group (JCPDS file no. 22–1086) (Naik and Hasolkar 2020). The inter-atomic d-spacing values are obtained by measuring the diameters of these concentric rings for studied nanoferrites. The inter-atomic d-spacing values corresponding to the (111) plane are 4.83Å and 4.97Å for CoFe_2O_4 and $\text{CoGd}_{0.10}\text{Fe}_{1.90}\text{O}_4$ nanoferrites, respectively. HRTEM micrograph at a high resolution of 10 nm also confirmed the crystalline uniformity of CoFe_2O_4 and $\text{CoGd}_{0.10}\text{Fe}_{1.90}\text{O}_4$ nanoferrites, see figures 5c and 5d, respectively. Thus, HRTEM microstructural analysis further established the phase purity and crystalline property in the spinel ferrite NPs within the fcc lattice (Praveen *et al.*, 2016; Nandan *et al.*, 2019; Choudhary *et al.*, 2021).

Magnetization analysis

The magnetic measurements of synthesized $\text{CoGd}_x\text{Fe}_{2-x}\text{O}_4$ ($x = 0$ to 0.10 with 0.02 interval) ferrites NPs were performed using the quantum design make SQUID down to 10K temperature and a maximum of ± 5 Tesla magnetic fields. Figure 6 (a-f) depicts the relation between magnetization and magnetic field, measured at various

constant temperatures of 20K, 100K, 200K, and 300K for all the $\text{CoGd}_x\text{Fe}_{2-x}\text{O}_4$ nanoferrites ($x = 0.0$ - 0.10, in an interval of 0.02). As the magnetization reaches the saturation edge, the perfect saturation occurs at the maximum field of ± 5 Tesla. It is evident from the isothermal M-H curves of all the studied samples that the nature of all the samples is hard ferromagnetic with high coercivity at 20 K. Insets of figure 6 (a-f) show an extensive view of the isothermal magnetization curve in the low magnetic field region around the origin for all the nanoferrites. From M-H curves, the saturation magnetization (M_s), coercivity (H_c), and remanent magnetization (M_r) amplitudes are illustrated in Table II for all the studied nanoferrites. Also, figure 7 shows the varied saturation magnetization, coercivity, and remanence magnetization at the different temperatures for the CoFe_2O_4 nanoferrites. It depicts that the coercivity, remanent, and saturation magnetization value monotonically increased with a temperature decrease from 300K to 20K. Furthermore, the saturation magnetization in Bohr magneton units (n_B) of the studied nanoferrites was calculated by the formula given below (Shirsath *et al.*, 2011; Lal *et al.*, 2020).

Table II. Magnetic parameters for $\text{CoGd}_x\text{Fe}_{2-x}\text{O}_4$ ($x = 0.0, 0.02, 0.04, 0.06, 0.08$ and 0.10) nano ferrites measured at different temperatures

T(K)	Gd Concentration (x) in $\text{CoGd}_x\text{Fe}_{2-x}\text{O}_4$								
	x=0.0			x=0.02			x=0.04		
	M_s (emu/g)	H_c (kOe)	M_r (emu/g)	M_s (emu/g)	H_c (kOe)	M_r (emu/g)	M_s (emu/g)	H_c (kOe)	M_r (emu/g)
300	70.7	1.21	23.7	73.0	1.22	20.2	40.4	1.18	9.9
200	75.5	3.56	38.5	77.2	3.27	32.1	43.6	2.95	16.3
100	76.0	9.05	51.8	78.9	9.10	48.1	44.5	8.34	26.0
20	78.5	13.4	58.8	79.1	14.6	55.1	45.2	13.96	30.2
T(K)	Gd Concentration (x) in $\text{CoGd}_x\text{Fe}_{2-x}\text{O}_4$								
	x=0.06			x=0.08			x=0.10		
	M_s (emu/g)	H_c (kOe)	M_r (emu/g)	M_s (emu/g)	H_c (kOe)	M_r (emu/g)	M_s (emu/g)	H_c (kOe)	M_r (emu/g)
300	48.5	1.25	14.0	45.2	0.98	10.1	42.1	1.04	9.5
200	52.3	3.30	23.0	49.3	2.80	17.1	45.8	2.67	15.2
100	53.8	9.12	33.3	51.0	8.50	27.9	47.9	8.00	24.9
20	55.8	14.6	38.2	53.8	14.7	33.9	51.9	13.8	30.7

Table III. Magnetic parameters for $\text{CoGd}_x\text{Fe}_{2-x}\text{O}_4$ ($x = 0.0, 0.02, 0.04, 0.06, 0.08$ and 0.10) nano-ferrites measured at room temperatures

Parameters	Gd Concentration (x) in $\text{CoGd}_x\text{Fe}_{2-x}\text{O}_4$					
	x = 0.0	x = 0.02	x = 0.04	x = 0.06	x = 0.08	x = 0.10
n_B (μ_B)	2.97	3.09	1.72	2.09	1.96	1.84
K ($\times 10^3$) emu Oe/g	87.2	90.8	48.6	61.8	45.2	44.6
M_r/M_s	0.33	0.27	0.24	0.28	0.22	0.22

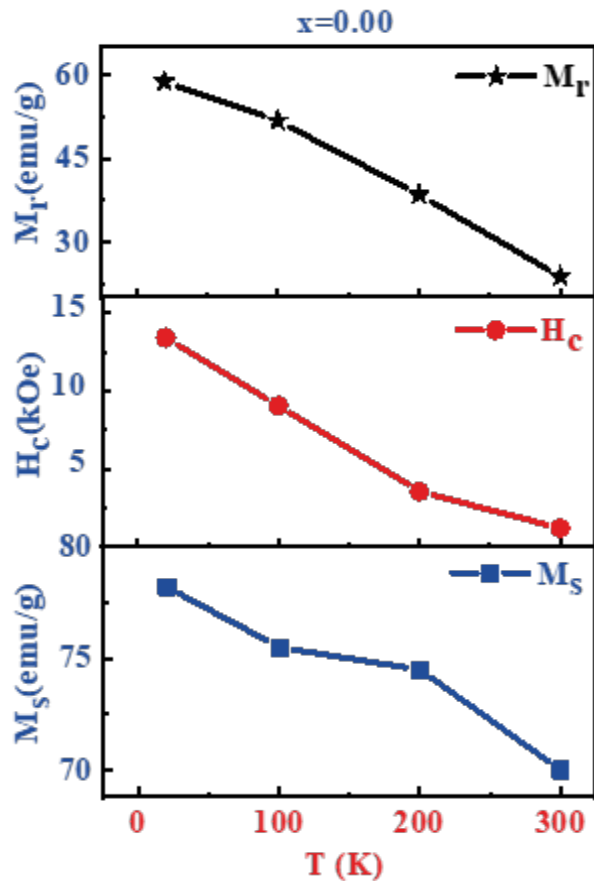


Fig. 7. Saturation magnetization M_s , Coercive field H_c , Remanent magnetization M_r versus temperature, for CoFe_2O_4 ($x=0.00$) sample

$$n_B = \frac{M_w \times M_s}{5585}$$

where M_w and M_s represents the molecular weight and saturation magnetization, correspondingly. As shown in Table III, overall decreasing behavior in the value of n_B was observed with increasing Gd^{3+} ions content.

The CoFe_2O_4 is an inverse spinel $[\text{Fe}^{3+}]_A [\text{Co}^{2+}\text{Fe}^{3+}]_B \text{O}_4$, and the whole Gd^{3+} preferentially occupies the octahedral B site mainly due to a larger ionic radius, which can be demonstrated as $[\text{Fe}^{3+}]_A [\text{Co}^{2+}\text{Gd}^{3+}_x \text{Fe}^{3+}_{(1-x)}]_B \text{O}_4$. The total magnetic moment (M) of the whole lattice is given by the formula $M = M_B - M_A$, where M_A and M_B are magnetic moments of A and B sublattices, correspondingly. In the magnetization process, A-A and B-B interactions are feeble compared to A-B interactions in the spinel lattice (Lal *et al.*, 2021). Therefore, the doping of Gd^{3+} ions on the B site reduces the magnetization of octahedral sublattices. Hence, net magnetization decreases on increasing Gd^{3+} concentration further, and hence the saturation magnetization reduces with a surge in Gd^{3+} content, as shown in figure 7 and Table II (Kadam *et al.*, 2020; Sahanashree *et al.*, 2018; George *et al.*, 2020). It is also clearly reflected in Table II that as Gd^{3+} content rises, coercivity (H_c) and remanence magnetization (M_r) values also decrease.

Additionally, temperature-dependent dc magnetization measurement has been accomplished within the temperature range of 300K to 10K in two modes, i.e., zero-field cooled (ZFC) mode and in field cooled (FC) mode under the influence of 100 Oe, 500 Oe, and 1000 Oe external applied magnetic fields were revealed in figure 8 (a-f) for $\text{CoGd}_x\text{Fe}_{2-x}\text{O}_4$ nanoferrites. From the figures, it can be seen that a considerable broadening in ZFC and FC curves confirmed that the relaxation mechanism of magnetic dipole moment occurred in all the samples (Aravind *et al.*, 2015). Furthermore, no blocking mechanism is found in ZFC mode up to room temperature, which suggests that all the samples are not superparamagnetic up to room temperature, which is also ascertained from their hysteresis curves. Furthermore, it can be concluded that the significant broadening in ZFC and FC protocol measurements confirmed the highly anisotropic nature of the synthesized nanoferrites (Kumar *et*

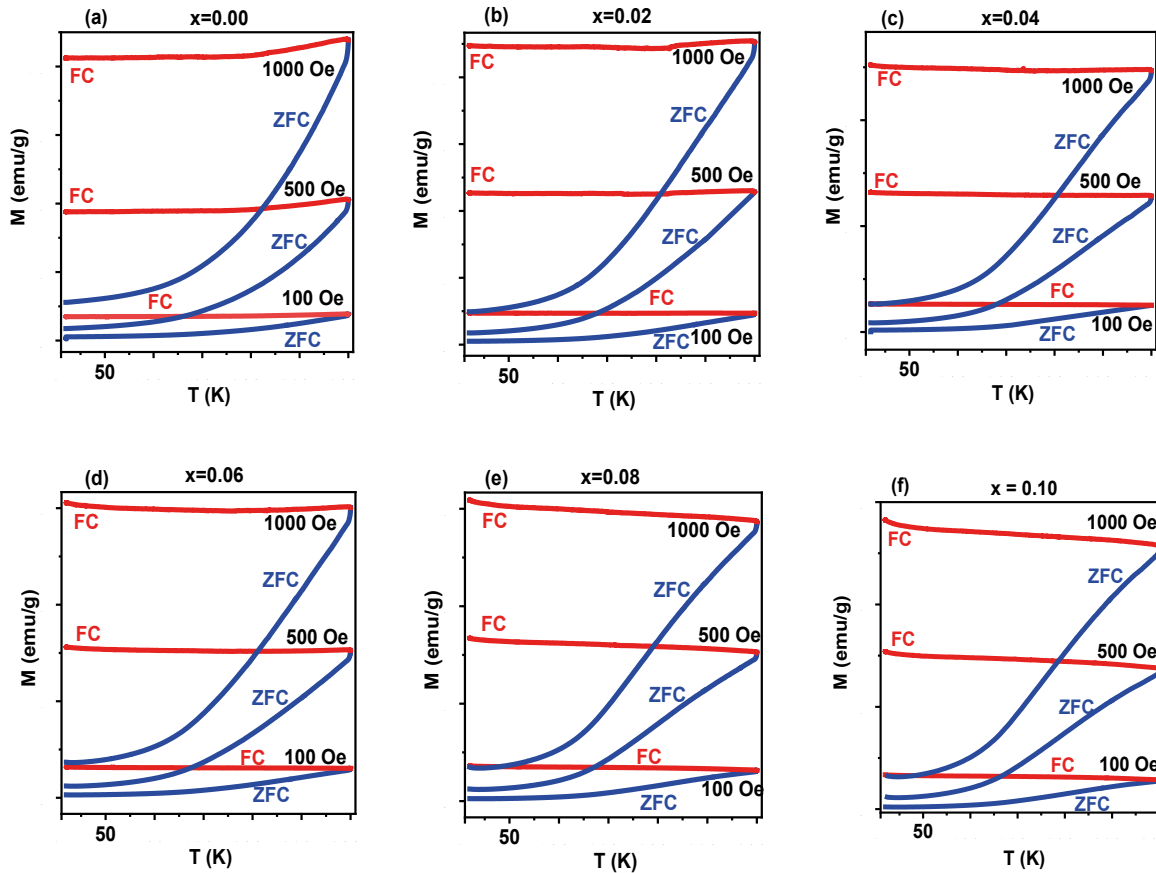


Fig. 8. FC-ZFC curves for different value of Gd ($x = 0.0, 0.02, 0.04, 0.06, 0.08$ and 0.10) in $\text{CoGd}_x\text{Fe}_{2-x}\text{O}_4$ nanoferrites

al., 2014). Moreover, figure 8 (a-f) reveals that the anisotropic nature is decreased with Gd doping in studied cobalt nanoferrites (Table III). Magneto crystalline anisotropy constant (K) was calculated by the formula $K = (M_s \times H_c) / 0.98$. The lower value of squareness ratio (SQR), as shown in Table III, indicates the easy reorientation of magnetization direction to the nearby, easy axis of magnetization. As observed in Table III, Gd doped Co nanoferrites samples have less SQR than pure Co nanoferrites (Assar *et al.*, 2015).

Optical band gap analysis

The UV-Vis spectroscopy inspected the Gd doped and undoped cobalt nanoferrites samples at room temperature at 200–800 nm. Figure 9 displays the Kubelka–Munk–Tauc plots of the Gd doped cobalt nanoferrites samples. The band-gap energies (E_g) were attained by extrapolating the

straight line of the plot of $[F(R)h\nu]^2$ versus $h\nu$ to $[F(R)h\nu]^2 = 0$ axis. The values of the direct optical band gap varied from 2.47 to 1.43 eV, as shown in figure 9. The band gap decreases with increasing Gd content in samples. Typically, band gap values rely on crystallite size, doping element, impurities etc. The declining nature of the band gap value in figure 9 can be understood based on the important part of Gd ($4f^7$) electrons in $\text{CoGd}_x\text{Fe}_{2-x}\text{O}_4$ ferrites NPs. These electrons can provide a donor state underneath the conduction band (C.B.) which supports the transfer of electrons from the lower energy valence band to higher energy C.B. via this state (Mansour *et al.*, 2020). Consequently, the optical band gap of $\text{CoGd}_x\text{Fe}_{2-x}\text{O}_4$ ferrites NPs shows a reducing tendency with Gd/Fe doping process. So, Gd^{3+} ions in the place of Fe^{3+} ions can regulate the energy band gap values of $\text{CoGd}_x\text{Fe}_{2-x}\text{O}_4$ ferrites NPs. To available literature, there is no report about band gap lessening related to CoFe_2O_4 ferrites NPs doped with Gd ions (Abdoa and El-Dalya, 2021).

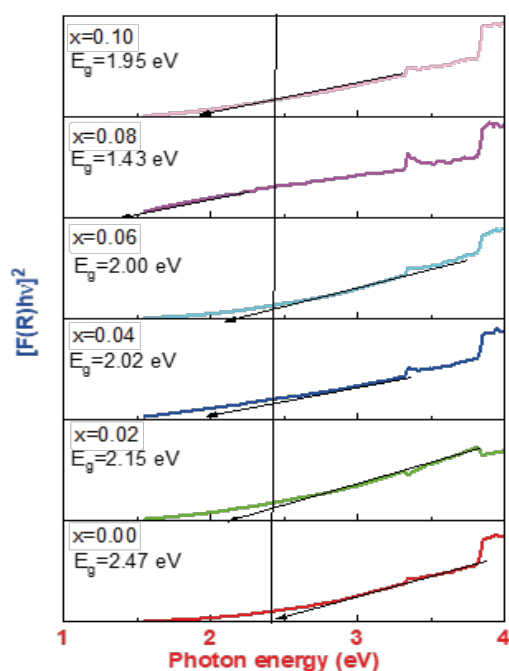


Fig. 9. Plots of $[F(R)hv]^2$ of $\text{CoGd}_x\text{Fe}_{2-x}\text{O}_4$ ferrites NPs with $x = 0.0, 0.02, 0.04, 0.06, 0.08$ and 0.10 . The linear extrapolation of $[F(R)hv]^2$ versus hv to $[F(R)hv]^2 = 0$ axis

Conclusion

We have successfully synthesized Gd doped cobalt nanoferrites series, i.e., $\text{CoGd}_x\text{Fe}_{2-x}\text{O}_4$, by the sol-gel self-combustion method. The XRD analysis established the effective place of the bigger rare-earth cations in the spinel environment. Moreover, XRD results confirmed the presence of single-phase ferrite NPs of $\sim 15\text{--}21$ nm sizes and crystallized in the cubic spinel structure. SEM images depicted the well-known nanostructure type morphology for all the studied samples. HRTEM results and SAED pattern show the studied samples' crystalline properties and phase purity, which reconfirmed the XRD outcome. Increasing Gd^{3+} concentration in studied cobalt ferrite NPs led to a reduction in average particle size. It may be attributed to internal lattice stress and bond energy of $\text{Gd}^{3+}\text{--O}^{2-}$ in nanoferrites. The magnetization measurements show that all the studied cobalt ferrite NPs are hard ferromagnetic within the temperature range of $300\text{--}20\text{K}$. In addition, magnetization measurements also showed that magnetic properties are highly sensitive with Gd doping in $\text{CoGd}_x\text{Fe}_{2-x}\text{O}_4$ ferrites NPs. Studies show that saturation magnetization, coercivity, and remanent magnetization values decrease with increased Gd^{3+} concentration. Moreover, Coercivity, remanent magnetization and saturation magnetization mono-

tonically increased with decreasing temperature from 300K to 20K . The optical band gap analysis shows that the band gap decreases with increased Gd content. This property may be used to improve the photocatalytic efficiency for water remediation. This study put cobalt ferrite NPs in significant materials for utilization in spintronics, photocatalysis, photovoltaics and optoelectronics. The present study revealed that structural and magnetic properties could be changed by monitoring the quantity of Gd in cobalt ferrite NPs.

Acknowledgment

The authors thank USIC, University of Rajasthan, Jaipur, for rendering the SQUID magnetometry and SEM facility. In addition, we thank Simran Sapra for help in collecting HRTEM data and CRF, IIT Delhi for providing the facility, and thanks to Banasthali Vidyapith, Banasthali, Rajasthan for the XRD facility.

References

- Abdoa MA and El-Dalya AA (2021), Sm-substituted copper-cobalt ferrite nanoparticles: Preparation and assessment of structural, magnetic and photocatalytic properties for wastewater treatment applications, *J. Alloy. Compd.* **883**: 160-796. DOI: [org/10.1016/j.jallcom.2021.160796](https://doi.org/10.1016/j.jallcom.2021.160796)
- Amiri M, Salavati-Nisari M and Akbari A (2019), Magnetic nanocarriers: Evolution of spinel ferrites for medical applications, *Adv. Colloid Interface Sci.* **265**: 29-44. DOI: [org/10.1016/j.cis.2019.01.003](https://doi.org/10.1016/j.cis.2019.01.003)
- Anwar A, Yousuf MAY, Zulfiqar S, Agboola PO, Shakir I, Al-Khalli NF and Warsi MF (2021), The impact of highly paramagnetic Gd^{3+} cations on structural, spectral, magnetic and dielectric properties of spinel nickel ferrite nanoparticles, *Journal of Saudi Chemical Society.* **25**(9): 101-306. DOI: [org/10.1016/j.jscs.2021.101306](https://doi.org/10.1016/j.jscs.2021.101306)
- Aravind G, Raghasudha M and Ravinder D (2015), Synthesis, characterization and FC-ZFC magnetization studies of cobalt substituted lithium nano ferrites, *Journal of Magnetism and Magnetic Materials* **378**: 278-284. DOI: [org/10.1016/j.jmmm.2014.11.052](https://doi.org/10.1016/j.jmmm.2014.11.052)
- Assar ST, Abosheishah HF, Saafan SA and El Nimr MK (2015), Preparation, characterization and magnetization of nano and bulk $\text{Ni}_{0.5}\text{Co}_{0.5-2x}\text{Li}_x\text{Fe}_{2+x}\text{O}_4$ samples, *J. Mol. Strut.* **1084**: 128-134. DOI: [10.1007/s11356-022-21688-8](https://doi.org/10.1007/s11356-022-21688-8)
- Chejara U, Prajapati A and Kumar A (2022), Dielectric studies for rare earth doped magnesium ferrite material. *Environ, Sci. Pollut. Res.*

- Choudhary BL, Kumari N, Kumari J, Kumar A and Dolia SN (2021), Relaxation mechanism in $\text{Ni}_{0.5}\text{Zn}_{0.5}\text{Fe}_2\text{O}_4$ nanocrystalline ferrite at a lower temperature, *Materials Letters*. **304**: 130-731. DOI: [org/10.1016/j.matlet.2021.130731](https://doi.org/10.1016/j.matlet.2021.130731)
- Cullity BD and Stock SR (1978), Elements of X-ray Diffraction in Diffraction III: Real Samples, 3rd Ed. 170 Addison-Wesley, Boston. Chap. 5. DOI: [org/10.1002/cssc.202000932](https://doi.org/10.1002/cssc.202000932)
- Debnath B, Parvin S, Dixit H and Bhattacharyya S (2020), Oxygen-defect-rich cobalt ferrite nanoparticles for practical water electrolysis with high activity and durability, *Chem Sus Chem*. **15**: 3875-3886. DOI: [org/10.1002/cssc.202000932](https://doi.org/10.1002/cssc.202000932)
- Dhiman M and Singhal S (2019), Enhanced catalytic properties of rare-earth substituted cobalt ferrites fabricated by sol-gel auto-combustion route, *Materials Today: Proceedings*. **14**: 435-444. DOI: [org/10.1016/j.matpr.2019.04.166](https://doi.org/10.1016/j.matpr.2019.04.166)
- Dippong T, Levei EA and Cadar O (2021), Recent Advances in synthesis and applications of MFe_2O_4 (M = Co, Cu, Mn, Ni, Zn) nanoparticles, *Nanomaterials*. **11**: 15-60. DOI: [org/10.3390/nano11061560](https://doi.org/10.3390/nano11061560)
- George LCV, Maheen M and Mohammed EM (2020), Enhanced magnetic properties at low temperature of Mn substituted Ni-Zn mixed ferrite doped with Gd ions for magnetoresistive applications, *Materials Research Bulletin* **126**: 110-833. DOI: [org/10.1016/j.materresbull.2020.110833](https://doi.org/10.1016/j.materresbull.2020.110833)
- Goldman A (1999), Handbook of Modern Ferromagnetic Materials. *Kluwer Academic Publishers*, Norwell, Massachusetts, USA. DOI: [org/10.1007/978-1-4615-4917-8](https://doi.org/10.1007/978-1-4615-4917-8)
- Issa B, Obaidat IM, Albiss BA and Haik Y (2013), Magnetic nanoparticles: surface effects and properties related to biomedicine applications, *Int. J. Mol. Sci*. **14**: 21266-21305. DOI: [org/10.3390/ijms141121266](https://doi.org/10.3390/ijms141121266)
- Jahan N, Khan MNI and Khandaker JI (2021), Exploration through structural, electrical, and magnetic properties of Al^{3+} doped Ni-Zn-Co nanospinel ferrites, *ACS omega*. **48**: 32852-32862. DOI: [org/10.1021/acsomega.1c04832](https://doi.org/10.1021/acsomega.1c04832)
- Jiang J and Yang YM (2009), Effect of Gd substitution on structural and magnetic properties of Zn-Cu-Cr ferrites prepared by novel rheological technique, *Materials Science and Technology* **25**: 415-418. DOI: [org/10.1179/174328408X296006](https://doi.org/10.1179/174328408X296006)
- John J, Dhananjaya M, Suresh S, Savitha Pillai S, Sahoo M, Hussain OM, Philip R and Mahadevan Pillai VP (2020), Effect of manganese doping on the structural, morphological, optical, electrical and magnetic properties of BaSnO_3 , *J Mater Sci: Mater Electron* **31**: 11159-11176. DOI: [org/10.1007/s10854-020-03665-4](https://doi.org/10.1007/s10854-020-03665-4)
- Kadam AB, Mande VK, Kadam SB, Kadam RH, Shirsath SE and Borade RB (2020), Influence of gadolinium (Gd^{3+}) ion substitution on structural, magnetic and electrical properties of cobalt ferrites, *Journal of Alloys and Compounds* **840**: 155-669. DOI: [org/10.1016/j.jallcom.2020.155669](https://doi.org/10.1016/j.jallcom.2020.155669)
- Klein L, Aparicio M and Jitianu A (2018), Handbook of Sol-Gel Science and Technology Processing, characterization and applications, *Cham Springer International Publishing*. DOI: [org/10.1007/978-3-319-32101-1](https://doi.org/10.1007/978-3-319-32101-1)
- Kumar L, Kumar P, Srivastava SK and Kar M (2014), Low Temperature and High Magnetic Field Dependence and Magnetic Properties of Nanocrystalline Cobalt Ferrite, *J. Supercond. Nov. Magn.* **27**: 7. DOI: [10.1007/s10948-014-2519-y](https://doi.org/10.1007/s10948-014-2519-y)
- Kumar R, Kumar H and Kumar M (2015), Enhanced saturation magnetization in cobalt doped Ni-Zn ferrite nanoparticles, *J. Supercond. Nov. Magn.* **28**: 3557-3564. DOI: [10.1007/S10948-015-3192-5](https://doi.org/10.1007/S10948-015-3192-5)
- Lal G, Punia K, Bhoi H, Dolia SN, Choudhary BL, Alvi PA and Dalela S (2021), Exploring the structural, elastic, optical, dielectric and magnetic characteristics of Ca^{2+} incorporated superparamagnetic $\text{Zn}_{0.5-x}\text{Ca}_{0.1}\text{Co}_{0.4+x}\text{Fe}_2\text{O}_4$ ($x = 0.0, 0.05 \& 0.1$) nanoferrites, *Journal of Alloys and Compounds*. **886**: 161-190. DOI: [org/10.1016/j.jallcom.2021.161190](https://doi.org/10.1016/j.jallcom.2021.161190)
- Lal G, Punia K, Dolia SN, Alvi PA, Choudhary BL and Kumar S (2020), Structural, cation distribution, optical and magnetic properties of quaternary $\text{Co}_{0.4+x}\text{Zn}_{0.6-x}\text{Fe}_2\text{O}_4$ ($x = 0.0, 0.1$ and 0.2) and Li doped quinary $\text{Co}_{0.4+x}\text{Zn}_{0.5-x}\text{Li}_0.1\text{Fe}_2\text{O}_4$, *Journal of Alloys and Compounds*. **828**: 154-388. DOI: [org/10.1016/j.jallcom.2020.154388](https://doi.org/10.1016/j.jallcom.2020.154388)
- Lal G, Punia K, Dolia SN, Alvi PA, Dalela S and Kumar S (2019), Rietveld refinement, Raman, optical, dielectric, Mössbauer and magnetic characterization of superparamagnetic fcc- CaFe_2O_4 nanoparticles, *Ceramics International* **45**(5): 5837-5847. DOI: [org/10.1016/j.ceramint.2018.12.050](https://doi.org/10.1016/j.ceramint.2018.12.050)
- Lin Q, Lin J, He Y, Wang R and Dong J (2015), The structural and magnetic properties of gadolinium doped CoFe_2O_4 nanoferrites, *Journal of Nanomaterials*, pp 294-239. DOI: [org/10.1155/2015/294239](https://doi.org/10.1155/2015/294239)
- Mansour SF, Al-Wafi R and Abdo MA (2020), Zn-Mg-La nanoferrites for storage and high frequency devices with augmenting the photocatalytic performance, *J. Alloy. Compd.* **826**: 154-125. DOI: [10.1016/j.jallcom.2020.154125](https://doi.org/10.1016/j.jallcom.2020.154125)

- Menezes PW, Panda C, Walter C, Schwarze M and Driess MA (2019), Cobalt-based amorphous bifunctional electro-catalysts for water-splitting evolved from a single-source lazulite cobalt phosphate, *Adv. Func. Mater.* **29**: 180-8632. DOI: org/10.1002/adfm.201808632
- Murugesan C and Chandrasekaran G (2015), Impact of Gd³⁺ substitution on the structural, magnetic and electrical properties of cobalt ferrite nanoparticles, *RSC Adv.* **5**: 73714-73725. DOI: org/10.1039/C5RA14351A
- Mykhailovych V (2021), Structural, optical, and catalytic properties of MgCr₂O₄ spinel-type nanostructures synthesized by Sol-gel auto-combustion method, *Catalysts.* **11**: 14-76.
- Naik PP and Hasolkar SS (2020), Consequence of B-site substitution of rare earth (Gd³⁺) on electrical properties of manganese ferrite nanoparticles, *J Mater Sci: Mater Electron.* **31**: 13434-13446.
- Nandan B, Bhatnagar MC and Kashyap SC (2019), Cation distribution in nanocrystalline cobalt substituted nickel ferrites: X-ray diffraction and Raman spectroscopic investigations, *J. Phys Chem. Solid.* **129**: 298-306.
- Palanisamy S and Wang YM (2019), Superparamagnetic iron oxide nanoparticulate system: synthesis, targeting, drug delivery and therapy in cancer, *Dalton Trans.* **48**: 9490-9515. DOI: org/10.1039/C9DT00459A
- Parvin S, Kumar A, Ghosh A and Bhattacharyya S (2020), An earth-abundant bimetallic catalyst coated metallic nanowire grown electrode with platinum-like pH-universal hydrogen evolution activity at high current density, *Chem. Sci.* **11**: 3893-3902.
- Patta GR, Babu VC and Kumar VR (2021), Study on the influence of gelation promoter on the structural and magnetic properties of cobalt ferrite nanoparticles developed through sol-gel method, *J. Sol-Gel Sci. Technol.* **100**: 310-325. DOI: org/10.1007/s10971-021-05647-2
- Pervaiz E and Gul IH (2012), Structural, electrical and magnetic studies of Gd³⁺ doped cobalt ferrite nanoparticles, *International Journal of Current Engineering and Technology* **2**(4): 2277-4106.
- Praveena K, Sadhana K and Liu HL (2016), Effect of Zn substitution on structural, dielectric and magnetic properties of nanocrystalline Co_{1-x}Zn_xFe₂O₄ for potential high density recording media, *J Mater Sci: Mater Electron* **27**: 12680-12690.
- Reddy DH and Yun YS (2016), Spinel ferrite magnetic adsorbents: Alternative future materials for water purification, *Coord. Chem. Rev.* **315**: 90-111. DOI: org/10.1016/j.ccr.2016.01.012
- Riaz A, Khan MA, Junaid M, Gulbadan S, Manzoor A, Ejaz SR, Ashraf GA, Somaily HH, Morsi M and Alshahrani T (2022), Effect of Nd³⁺ ions on structural, spectral, magnetic, and dielectric properties of Co-Zn soft ferrites synthesized via sol-gel technique, *Materials Chemistry and Physics.* **190**: 126-519
- Sahanashree BM, Melagiriappa E, Veena M and Shankaramurthy GJ (2018), Influence of Neodymium and gamma rays irradiation on structural electrical and magnetic properties of Co-Zn nanoferrites, *Mater. Chem. Phys.* **214**: 143-153. DOI: org/10.1016/j.matchemphys.2018.04.094
- Samariya A, Dolia SN, Prasad AS, Sharma PK., Pareek SP, Dhawan MS and Kumar S (2013), Size dependent structural and magnetic behaviour of CaFe₂O₄, *Current Applied Physics.* **13**: 8-30.
- Satyanarayana L, Reddy KM and Manorama SV (2003), Nano-sized spinel NiFe₂O₄: a novel material for the detection of liquefied petroleum gas in air, *Mater. Chem. Phys.* **82**: 21. DOI: org/10.1016/S0254-0584(03)00170-6
- Schloemann E (2000), Advances in ferrite microwave materials and devices, *Journal of Magnetism and Magnetic Materials.* **209**: 15-20.
- Sharma S, Verma MK, Sharma ND, Choudhary N, Singh S and Singh D (2021), Rare-earth doped Ni-Co ferrites synthesized by Pechini method: Cation distribution and high temperature magnetic studies, *Ceramics International.* **15**: 17510-17519.
- Shirsath SE, Jadhav SS, Toksha B, Patange S and Jadhav K (2011), Influence of Ce⁴⁺ ions on the structural and magnetic properties of NiFe₂O₄, *J. Appl. Phys.* **110**: 13-914. DOI: org/10.1063/1.3603004
- Su J, Xue H, Gu M, Xia H and Pan F (2014), Synthesis of spherical Cr₂O₃ nanoparticles by a microwave refluxing method and their photocatalytic properties, *Ceramics International.* **40**(9): 15051-15055.
- Valenzuela R (2012), Novel Applications of Ferrites, *Phys. Res. Int.*, pp 1-9. DOI: org/10.1155/2012/591839
- Zeng X, Zhang J, Zhu S, Deng X, Ma H, Zhang J, Zhang Q, Li P, Xu D, Mellors N, Zhang X and Peng Y (2017), Direct observation of cation distributions of ideal inverse spinel CoFe₂O₄ nanofibres and correlated magnetic properties, *Nanoscale.* **9**: 22. DOI:10.1039/C7NR02013A
- Zhao L, Cui Y, Yang H, Yu L, Jin W and Feng S (2006), The magnetic properties of Ni_{0.7}Mn_{0.3}Gd_xFe_{2-x}O₄ ferrite, *Materials Letters.* **60**: 104-108. DOI:10.1016/j.matlet.2005.07.083